Thermocapillary actuation of binary drops on solid surfaces

Yuejun Zhao, Fangjie Liu, and Chuan-Hua Chen[a)]
Department of Mechanical Engineering and Materials Science, Duke University, Durham, North Carolina 27708, USA

On hydrophobic solid surfaces, aqueous drops are typically not conducive to thermocapillary actuation. This letter reports thermal mobilization of water drops by encapsulating them with a long-chain alcohol. On a parylene-coated silicon substrate, a water-heptanol binary drop can assume a unique shape: the dome-shaped water drop is capped by a layer of heptanol, and the heptanol cap protrudes through a "foot" to a precursor film. For intermediate drop diameters, the speed of the binary drop is linearly proportional to its diameter and the imposed temperature gradient, with an offset accounting for the hysteresis force. © 2011 American Institute of Physics. [doi:10.1063/1.3632041]

Thermocapillary actuation offers the potential advantage of directly and controllably accessing aqueous samples[1] important for most biomedical and many industrial applications. Thermal mobilization of aqueous drops has been achieved in fluidic channels[2,3] and on liquid[4,5] and solid substrates.[6] Because of the partially non-wetting state of aqueous samples on most solid substrates, the thermocapillary motion may be hindered by large contact angle[7,8] and/or significant hysteresis.[8,9] As a result, thermocapillary actuation on open solid surfaces typically involves organic liquids on hydrophobic surfaces.[8–11] To thermally actuate aqueous drops on solid surfaces, hydrophilic substrates (e.g., silicon dioxide in Ref. 6) are used but the high-energy surfaces are prone to contamination. Here, we report thermocapillary actuation of a water drop on a hydrophobic solid surface by encapsulating it with a long-chain alcohol and thermally driving the binary drop (Fig. 1).

The silicon substrate ($20 \times 20 \times 0.5$ mm^3) was coated with a 1 μm-layer of parylene C (Specialty Coating Syst. PDS2010). A linear temperature gradient was established with two thermoelectric modules attached to the substrate by thermal grease. The surface temperature was measured by infrared imaging (FLIR A325) on a dummy wafer coated with a spray paint of known emissivity (Krylon flat white), and the temperature gradient was measured to be uniform in the 16 mm-long interspace between the two modules. Three temperature gradients, 1.2, 1.7, and 2.5 °C/mm (K/mm), were used with the average (midpoint) temperature fixed at 55 ± 2 °C. The working fluids were deionized water and 1-heptanol (Alfa Aesar A12793). The drop motion was monitored with a camera (Phantom V7.3) through a long-distance microscope (Infinity K2). The optical axis was at a 3° or 20° angle from the substrate surface.

A representative process of the thermocapillary actuation of the binary drop is shown in Fig. 2. The left column is a bird's eye view of the drop shape, while the right column is a side view (with a slight tilt angle of 3°, so that the mirror image can be used to pinpoint the solid surface). The imposed temperature gradient was 2.5 K/mm with the right being the cold side. First, a 3.4 μL water drop was placed on the parylene-coated silicon surface. The pure water drop would remain stuck on the surface indefinitely, as the contact angle hysteresis of a water drop on the parylene surface was up to 40°. Then, a 0.4 μL drop of pure heptanol was placed on the surface at the left (hotter) side of the water drop. Three stages were observed in Fig. 2:

Stage (a): Thermocapillarity drove the heptanol drop toward the water drop. Although the macroscopically visible drops merged at 0 s, a precursor film[12] of heptanol should have reached the water drop much earlier. The precursor film can be inferred from the decreasing contact angle of the water drop (see Supplemental videos, Fig. 2).

Stage (b): After a brief transient (within 0.1 s), a heptanol film enclosed the entire water drop, and the binary drop assumed the unique "cap-foot" shape (Fig. 1).

Stage (c): The binary drop was driven to the cold side and reached a steady-state velocity within 0.5 s, except for slight changes due to evaporation. A heptanol tail persisted behind the binary drop, as a very small amount was needed to encapsulate the water drop.

To confirm that, Fig. 1 indeed represents the physical picture of the binary drop in stage (c), three corroborating experiments were conducted: (1) The contact angle of a water drop on the parylene-coated substrate immersed in a heptanol bath at 55 °C was measured as 150°. The same water/heptanol contact angle was assumed for the inner drop in Fig. 1, which was supported by dual-band fluorescence imaging with different particles seeding the two liquids. (2) Additional heptanol was deposited on top of the cap of the binary drop. The extra heptanol floated on the surface as tiny
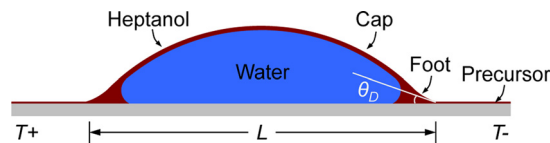

FIG. 1. (Color online) Schematic of a water-heptanol binary drop driven by a thermal gradient imposed on a solid substrate, with the thickness of the heptanol layer exaggerated. The dome-shaped water drop is enclosed by a heptanol cap, and the cap joins a precursor film through a heptanol "foot." The dynamic contact angle (θ_D) measures the nominal contact angle between the foot and the precursor. The diameter of the binary drop, L, measures the visible footprint of the binary drop as the precursor film is not optically visible.

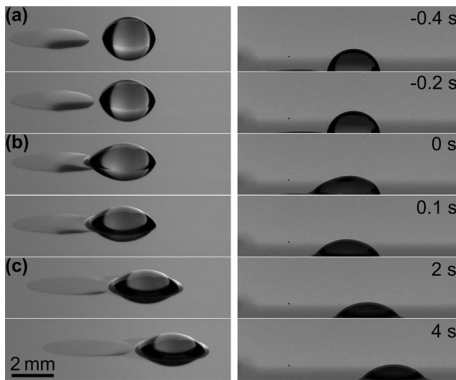a)Electronic mail: chuanhua.chen@duke.edu.

FIG. 2. Thermocapillary actuation of a binary heptanol-water drop. Stage (a): heptanol spread against the temperature gradient of 2.5 K/mm; Stage (b): heptanol and water drop mixed together; Stage (c): the binary drop was driven to the cold side. Left and right columns were captured in two independent experiments at a viewing angle of 20° and 3°, respectively. The center of the water drop was initially about 3 mm to the left of the midpoint. Time 0 corresponds to the point of merging of the *visible* parts of the heptanol and water drops. See supplemental videos S1, S2 (enhanced online) [URL: http://dx.doi.org/10.1063/1.3632041.1; http://dx.doi.org/10.1063/1.3632041.2].

droplets, but the shape of the binary drop was not altered by these additional droplets, suggesting that the binary drop was already covered with heptanol. (3) The binary drop was gently blown by compressed air. Although the center (water) portion could be easily blown dry, a (heptanol) ring around the dry spot was always left behind. The configuration in Fig. 1 is, therefore, reasonable considering that long-chain alcohols are surfactants for water.

The speed of thermocapillary actuation was measured as a function of the initial volume of the water drop (Fig. 3). To minimize the effect of evaporation, the speed was measured shortly after the binary drop velocity reached steady state (between 2 s and 4 s). Although the binary drop initiated with 0.2 μL heptanol consistently yielded slightly lower velocity than the control case with 0.4 μL, the overall trend was very similar for both cases. This observation suggested that the volume of heptanol played a minor role in determining the velocity, as long as there was sufficient heptanol to encapsulate the water drop. (As discussed below, the smaller velocity is related to the smaller diameter of the binary
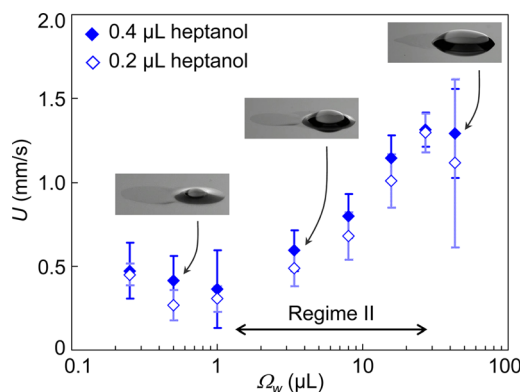
drop.) At a fixed temperature gradient, the velocity variation with the initial water volume (Ω_w) fell into three regimes:

Regime I: $\Omega_w \lesssim 1 \mu$L, where the overall motion was dominated by the heptanol puddle. In regime I, the speed of the binary drop decreased as the water volume increased, indicating that the water drop hindered the motion of the pure heptanol drop.

Regime II: 1μL $\lesssim \Omega_w \lesssim 30 \mu$L, where the binary drop took on the cap-foot shape as sketched in Fig. 1. In regime II, the speed increased monotonically with the water volume. It is remarkable that the speed of the binary drop was higher than either of its individual components (the water drop was initially stuck).

Regime III: $\Omega_w \gtrsim 30 \mu$L, where the velocity of large binary drops fell off the monotonic trend of regime II. In regime III, the large volume of water requires a larger amount of heptanol for complete encapsulation. In addition, gravitational effects become significant.

We shall now focus on regime II in which medium-sized water drops were thermocapillary-actuated *via* encapsulation with a minute amount of heptanol. In regime II, the speed (U) increased linearly with the contact diameter (L) of the binary drop (Fig. 4). The speed measured at different temperature gradients extrapolated to the same point on the vertical axis ($-U_H$). In the inset of Fig. 4, the linear-regime velocities collapsed onto a single curve, $U = \beta_T^{\mathrm{ex}}(dT/dx)L - U_H^{\mathrm{ex}}$, where $(dT/dx)L$ is the characteristic temperature difference across the drop. Extracted from the collapsed line, $\beta_T^{\mathrm{ex}} = 0.089$ mm s^{-1}K^{-1} and $U_H^{\mathrm{ex}} = 0.23$ mm/s.

These results are strikingly similar to the findings in Ref. 8, even though the systems under study are quite different: our's is a binary drop with a precursor film, while Brzoska *et al.*'s is a pure fluid without a precursor film. We shall rationalize our results by extending the model of Brochard and co-workers[7,8] for a slender 2D liquid ridge surrounded by a precursor film (Fig. 1). *From hereon, all material properties are those of heptanol unless otherwise specified.*

The precursor film brought about an important simplification of the (equilibrium) spreading coefficient, $S = 0$, because the "solid-vapor interface" was actually covered
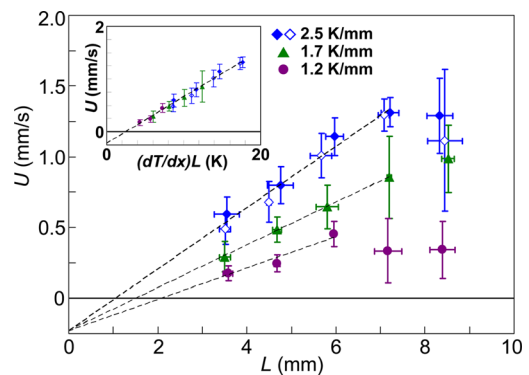

FIG. 3. (Color online) Steady-state speed (U) of the binary drop as a function of the water volume (Ω_w) at 2.5 K/mm. For pure heptanol without any water, the speed measured at the visible front edge was 0.59 mm/s for 0.4 μL and 0.45 mm/s for 0.2 μL. For consistency, the initial location of the water and heptanol drops was kept the same as in Fig. 2. In regime II, the velocity increases monotonically with the water volume.

FIG. 4. (Color online) Binary drop speed (U) as a function of the outer contact diameter (L). The heptanol volume was 0.4 μL except for an additional case with 0.2 μL at 2.5 K/mm. The dashed lines fitting the linear trends converge at a single point on the velocity axis, $-U_H^{\mathrm{ex}} = -0.23$ mm/s. When plotted against the nominal temperature difference across the binary drop, $(dT/dx)L$, all the data in the linear regime collapsed on the same line with an R^2 value of 0.990, yielding a coefficient of thermocapillary actuation $\beta_T^{\mathrm{ex}} = 0.089$ mm s^{-1}K^{-1}.

with a thin film of heptanol.[12] The balance between the driving and drag forces reads

$$\frac{d\gamma}{dx}L \sim \frac{6\eta\ell_n}{\theta_D}U - \frac{1}{2}\frac{d\gamma}{dx}L + f_\delta, \tag{1}$$

where $d\gamma/dx$ is the gradient of surface tension induced by the temperature gradient across a drop of contact diameter L, η is the viscosity, ℓ_n is a logarithmic factor that is usually between 10–20,[8,12] θ_D is the dynamic contact angle of the heptanol foot (see Fig. 1), and f_δ accounts for the hindering forces, including that due to the physical contact between the water drop and the solid substrate. The left hand term in Eq. (1) is the Marangoni stress exerted on the drop by the precursor film (of heptanol), which is different from Brzoska *et al.*[8] with a dry surrounding surface. The first term on the right accounts for the viscous drag which is dominated by the region near the dynamic triple contact line (of heptanol).[12] The second term on the right can be viewed as an additional driving force due to the Marangoni stress on the cap and the foot (at the air/heptanol interface), where the factor of 1/2 results from a lubrication approximation.[7,8] Rearranging Eq. (1),

$$U \sim \left(\frac{\theta_D}{4\ell_n}\frac{\gamma}{\eta}\frac{1}{\gamma}\frac{d\gamma}{dT}\right)\frac{dT}{dx}L - \frac{\theta_D}{6\ell_n}\frac{f_\delta}{\eta} = \beta_T\frac{dT}{dx}L - U_H. \tag{2}$$

The thermal actuation coefficient (β_T) can be estimated by plugging in Eq. (2): $\theta_D = 0.35$ (approximately 20° as in Fig. 2), $\gamma = 2.4 \times 10^{-2}$ N/m, $\gamma/\eta = 10.2$ m/s, and $(d\gamma/dT)/\gamma = 3.5 \times 10^{-3}$ K^{-1} (based on literature values at 55 °C (Refs. 13 and 14)), and assuming a reasonable value of $\ell_n \approx 15$,[8,12] giving rise to $\beta_T \sim 2 \times 10^{-4}$ m s^{-1} K^{-1} which is on the same order as the experimental value of $\beta_T^{ex} = 0.89 \times 10^{-4}$ m s^{-1}K^{-1}. In addition, the dependence of β_T on the dynamic contact angle explains why the binary drop with a much larger θ_D moved faster than the pure heptanol drop (Fig. 3).

Based on Eq. (2), the hysteresis force can be assessed from the thermocapillary data by

$$f_\delta \sim \frac{3}{2}\frac{1}{\gamma}\frac{d\gamma}{dT}\frac{U_H}{\beta_T}\gamma. \tag{3}$$

Without any fitting parameter, $f_\delta = 0.32$ mN/m using measurements in Fig. 4, which is very close to an independent gravity-driven measurement of the hysteresis force as follows. On an initially horizontal substrate heated to 55 °C (without any temperature gradient), a water drop was first deposited and then a 0.4 μL heptanol drop was placed nearby. The heptanol spread and eventually encapsulated the water drop to assume the binary shape in Fig. 2(c). The substrate was attached to a goniometer (Edmund NT55-838) with the tilt angle changed at 0.1° increments, and the hysteresis force was given by the angle (α) leading to an incipient motion of the binary drop,[15]

$$f_\delta \approx \frac{2Mg\sin\alpha}{\pi L}, \tag{4}$$

where M is the mass of the binary drop and g is the gravitational acceleration. For the four volumes tested in regime II (Fig. 3), a hysteresis of $f_\delta = 0.37 \pm 0.07$ mN/m was obtained. There is an ambiguity in the length scale associated with the hysteresis force in Eq. (4). The contact diameter of water

(L_w) is perhaps more appropriate because the presence of water gave rise to measurable hysteresis. However, based on the bottom-up fluorescence imaging of parylene-coated glass, the difference between L and L_w was at most 20% for smaller volumes and diminished with increasing volume in regime II. Since this difference was comparable to the uncertainty of f_δ measurements, L was adopted for its ease of measurement.

Although overly simplified, our 2D scaling model assuming a slender liquid ridge agrees reasonably well with the experiments. Some of the limitations in the 2D steady-state model using an *ad hoc* incorporation of the hysteresis force[7,8] may be addressed by alternative models, see for example Refs. 9, 11,16–18. Another drawback of our current model is the negligence of the complex motion within the binary drop. Preliminary particle imaging indicated rich flow patterns within the water drop and near the water/heptanol/solid triple line, see for example related reports in Refs. 4 and 19. A more accurate 3D model should be developed to faithfully account for both components of the binary drop and their interaction with the solid surface, e.g., by extending the theoretical work of Greco and Grigoriev.[20]

Concerning practical applications involving thermocapillary actuation of aqueous samples, we have used the same binary actuation mechanism to drive water drops with other long-chain alcohol (e.g., octanol) and solid surfaces (e.g., gold-coated silicon). Although our encapsulation scheme introduces a precursor film (and possibly a tail) of a secondary fluid, cross contamination should not be a major problem because the primary drop (water here) seems to be completely encapsulated by the secondary driving fluid.

[1]A. Darhuber and S. Troian, Annu. Rev. Fluid Mech. **37**, 425 (2005).
[2]T. Sammarco and M. Burns, AIChE J. **45**, 350 (1999).
[3]Z. Jiao, N. Nguyen, and X. Huang, J. Micromech. Microeng. **17**, 1843 (2007).
[4]R. Grigoriev, M. Schatz, and V. Sharma, Lab Chip **6**, 1369 (2006).
[5]E. Yakhshi-Tafti, H. Cho, and R. Kumar, Appl. Phys. Lett. **96**, 264101 (2010).
[6]A. Darhuber, J. Valentino, S. Troian, and S. Wagner, J. Microelectromech. Syst. **12**, 873 (2003).
[7]F. Brochard, Langmuir **5**, 432 (1989).
[8]J. Brzoska, F. Brochard-Wyart, and F. Rondelez, Langmuir **9**, 2220 (1993).
[9]J. Chen, S. Troian, A. Darhuber, and S. Wagner, J. Appl. Phys. **97**, 014906 (2005).
[10]A. Darhuber, J. Valentino, J. Davis, S. Troian, and S. Wagner, Appl. Phys. Lett. **82**, 657 (2003).
[11]V. Pratap, N. Moumen, and R. Subramanian, Langmuir **24**, 5185 (2008).
[12]P. de Gennes, Rev. Mod. Phys. **57**, 827 (1985).
[13]R. Strey and T. Schmeling, Ber. Bunsenges. Phys. Chem. **87**, 324 (1983).
[14]*Handbook of Chemistry and Physics*, 91st ed., edited by W. Haynes (CRC, Boca Raton, 2011).
[15]E. Dussan and R. Chow, J. Fluid Mech. **137**, 1 (1983).
[16]M. Ford and A. Nadim, Phys. Fluids **6**, 3183 (1994).
[17]M. Smith, J. Fluid Mech. **294**, 209 (1995).
[18]J. Gomba and G. Homsy, J. Fluid Mech. **647**, 125 (2010).
[19]S. Rybalko, N. Magome, and K. Yoshikawa, Phys. Rev. E **70**, 046301 (2004).
[20]E. Greco and R. Grigoriev, Phys. Fluids **21**, 042105 (2009).